Diffusive representation modelling thermal and overvoltage for permanent magnet synchronous motor fed by voltage inverter

Ben Smida KHALED[1][*]**, Ben smida MONCEF**[2]**, Mrabet BRAHIME**[3],
[1]Department of Industrial Electronics, School of Engineering, University of Sousse, Sousse, Tunisia
[2]Electrical Department, National Institute of Applied Sciences and Technology INSAT, University of Carthage,
Tunis, Tunisia
[3]College of Engineering at Alkharj KSA, University Prince Sattam Bin Abdulaziz, Riyadh, Saudia Arabia

Abstract: Life of electric machines is very sensitive to temperature increases especially due to the fragility of their windings as well as to the overvoltage at the motor's terminals. Therefore, it is necessary to find the temperature in the most sensitive areas of the machine. It has been known for a long time that temperature rise is caused by the losses in the machine; thus, various models have been proposed. It has also been shown that the permanent magnet synchronous motor fed by a voltage inverter overheats more than the one supplied by a sinusoidal voltage. Indeed the permanent magnet synchronous motor fed by a voltage inverter deserves special attention. In this paper a new technique based on diffusive representation is used to develop two coupled mathematical models; one for thermal variation in some of the most delicate places of winding and another one for the overvoltage at the motor's terminals. The obtained simulations and experimental results show clearly the validity and the high performance of the proposed models.

Key words: Diffusive representation, inverter drive, overvoltage modeling, permanent magnet synchronous motor, thermal modeling

1. Introduction

The use of the permanent magnet synchronous motor is booming and seems to become unavoidable in the field of electric traction thanks to its high efficiency and high power density. Among others, these motors supplied by inverter must consider aging problems caused by overvoltage associated with the rise times [1], the nature of the load and the corresponding speeds. Indeed, cooling at low speeds with rated currents, which is usually done by ventilation, becomes insufficient leading to a significant heating of the machine. In addition, the voltages supplied by inverters still have nonsinusoidal waveforms, and even with passive filtering, the current is rich in harmonics. The presence of harmonics increases losses in the machine and leads to more severe thermal stresses due to overheating of the order 10% to 30% [2]. Influenced by temperature with or without the chemical action of the environment (oxygen, humidity, etc.), specific decomposition reactions of each material will intervene to progressively degrade the original characteristics of the product. Therefore, on winding insulation materials the following degradations: mass loss, thickness reduction, dielectric decrease and electrical resistivity decrease can be observed. Thermal stresses, sustained by an electric machine, strongly condition its life and may lead to deterioration of its performance. Respectively, the electrical and thermal models of an electrical machine can affect the power losses and the temperature fields. Such thermal models become more sophisticated due to

---

*Correspondence: elektrik@tubitak.gov.tr

advances in computing and measurement procedures. These models may allow the design of new machines with efficiency and improved heat dissipation. At any time, the monitoring system allows following the temperatures and overvoltage in an electrical machine. The design of this monitoring tool requires different skills. First, a mathematical model capable of restoring the transient thermal distributions of electrical machines should be built following the standards in thermal modeling. Second, electrical losses of machine should be determined based on electric equivalent scheme. Such a design should support the monitoring system to track the changing temperatures and losses in an electrical machine at any instant. Thermal modeling of electrical machines has been the subject of many studies, such as the nodal thermal model developed in [3–23]. Currently, research in thermal analysis using lumped parameter models [24–28] are focused on developing models that utilize different parameters of electrical motors.This technique supports studying the impacts of different parameters or thermal mode accuracy. Fluid flowing characteristics, including coolant and air gap [29–30], are studied. The coupling of the electromagnetic and thermal events is studied in [31,32]. Meanwhile, to reduce the order of the thermal model, cancellation of poles-zero, Hankel-singular-based models are employed [15]. Moreover, different thermal analyses using methods such as the finite element method (FEM) and finite-volume method have been widely studied [16–21]. However, the nature of the 3D thermal problem and difficulty associated with coolant heating have been presented among the drawbacks of using finite element thermal analysis techniques. As an alternative, diffusive representation schemes have emerged as easier and faster strategies to couple electrical and thermal models. Our study builds on this interesting new approach to model thermal and over voltage situations for permanent magnet synchronous motor fed by voltage inverters.
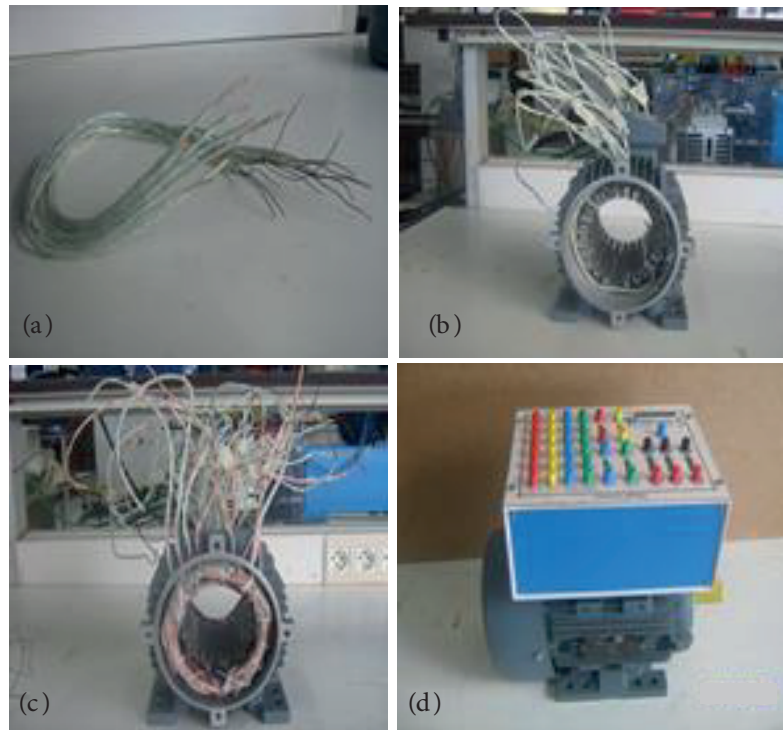
2. Instrumentation of the permanent magnet synchronous motor

Experimental results are obtained by means of the test bench of Figure 1, where necessary requirements for machine supply and signals measurements are provided. The machine under study is a 1.5 kW permanent magnet synchronous motor. Figure 2 shows the winding diagram of the stator, which are spread over 24 slots. To observe the voltage distribution in the winding, a phase has been equipped with five sensors welded on different coils. These sensors give direct access to the terminals of each coil and coil to ground voltages. Further, to measure the temperatures in the stator, the permanent magnet synchronous motor is equipped with NTC thermistors as shown in Figure 1.

3. Electrical model of the permanent magnet synchronous motor

Modeling of AC machines in the shape of an electrical lumped parameter model has been studied extensively. However, many of these models do not take into account the frequency response of the machine, especially for modern drive applications where the machine is fed by a voltage inverter. The most appropriate one is to consider the winding as a transmission line with losses. The model parameters are identified either by specific measurements or digital 2D or 3D techniques using FEM [1]. Figure 3 shows the localized-parameter transmission line of the permanent magnet synchronous motor phase.

In this model, R is resistive losses in the wire, R_{iron} is the iron frame losses, L is the inductance of the stator phase, C_c is the capacity representing the capacitive coupling between two motor windings, C_i is the capacitive coupling between winding and ground, and R_i is the resistance representing the dielectric between the coil and the ground. In order to simulate the behavior of the electrical model of the permanent magnet synchronous motor, it can be transformed into a functional diagram. In fact an equation of the currents is

Figure 1. Permanent magnet synchronous motor scheme with thermistor location (a): NTC thermistors; (b) and (c): location of thermistor in the end winding, slot winding and stator iron; (d): study motor equipped with NTC thermistors
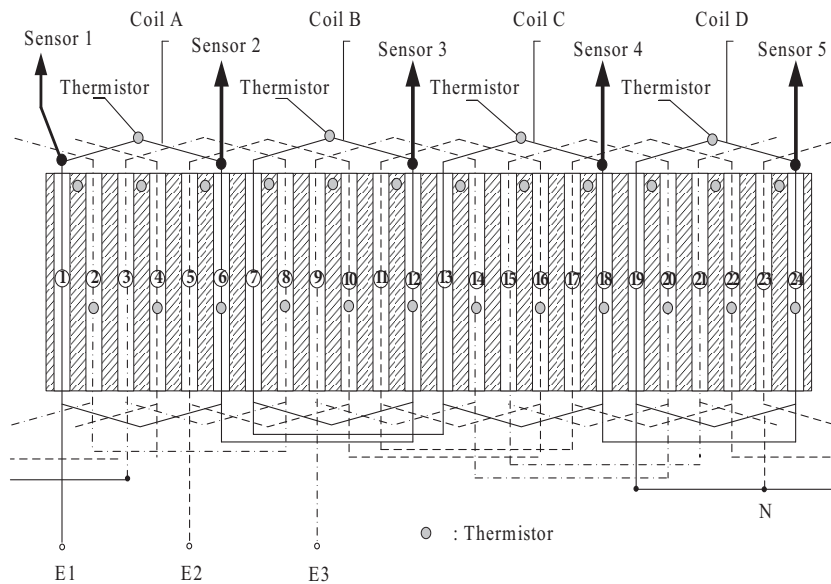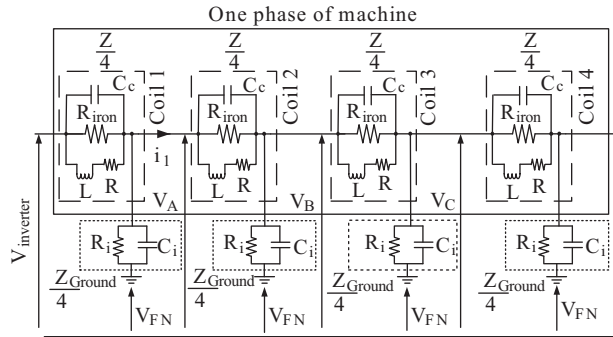

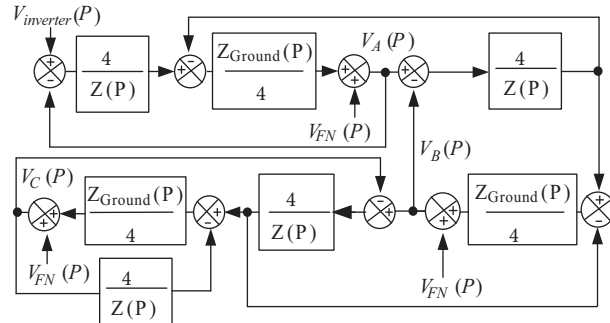**Figure 2**. Winding diagram of the stator

necessary. For example, the expression of the current i1 passing through the impedance Z is given by Eq. (1):

$$i_1 = 4\frac{V_A - V_B}{Z} = 4\frac{V_B - V_{FN}}{Z_{Ground}} + 4\frac{V_B - V_C}{Z}. \tag{1}$$

The same procedure as Eq. (1) is applied for the four coils; the functional diagram of a one phase is given in Figure 4.

Figure 3. Electrical model of the permanent magnet synchronous motor phase.

Figure 4. Functional diagram of permanent magnet synchronous motor phase.

The Z and Z_{Ground} elements can be experimentally determined using the knowledge of frequency behavior of the winding in two configurations: open line $Z_{in,nc}(jw)$, and shorted line $Z_{in,c}(jw)$. The machine is stopped; the measurements are made for a single phase and the two other phases have been disconnected. To do this, we use HP impedance analyzer; Figure 5 shows the block diagram of the two kinds of measurement. As presented in Figure 5a, $Z_{in,nc}(jw)$ can be measured when one terminal of winding is connected to HP impedance while the other terminal of the winding is disconnected. In addition, the frame of the machine is connected to terminal of the analyzer. Similarly, as presented in Figure 5b, one terminal of winding is connected to HP impedance while the other terminal of the winding is connected to both the frame and other terminal of the analyzer. All the impedances measurements were made for different states of heating of the machine. After each impedance measurement, the machine is heated using an electric furnace.

The frequency response of the phase characteristic impedance Zc can be described via Eq. (2).

$$Z_c = \sqrt{Z_{in,c}.Z_{in,nc}}, \tag{2}$$

where $Z_{in,c}$ can be expressed as:

$$Z_{in,nc} = \sqrt{Z.Z_{Ground}} \coth \sqrt{\frac{Z}{Z_{Ground}}}. \tag{3}$$

At low frequency, $\sqrt{\frac{Z}{Z_{Ground}}}$ tends to be zero. Therefore, for sufficiently small frequencies the impedance could be described using: $\coth \sqrt{\frac{Z}{Z_{Ground}}} \cong \sqrt{\frac{Z_{Ground}}{Z}}$.

Then, Eq. (2) becomes:

$$Z_{in,c} = Z_{Ground}. \tag{4}$$

According the established expression for the characteristic impedance Z_c, it is possible to calculate the impedance Z by the following relationship:

$$Z = \frac{Z^2}{Z_{Ground}}. \tag{5}$$

Furthermore, the models can be used to describe the impedance winding Z and Z_{Ground} subject to induce by the variation in frequency. Foster models are usually referred to as the lumped circuit model parameter RL, which could be obtained by identifying the frequency winding measures. Adaptive models obtained in this way should be of infinite order sufficient to exactly reproduce the impedance to all frequencies. Thus, for a frequency range set beforehand, the developed model reproduces exactly the frequency response measured or simulated by FEM, while the response will not be perfect for other frequencies. A recent tool, the diffusive representation supports representation of states for nonrational transfer functions. The diffusive symbol β of input-output operator Z in Figure 6 is given in Eq. (6).

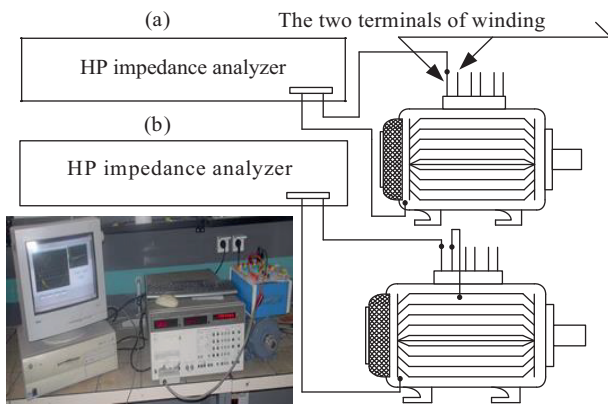$$Y(P) = \int_0^{+\infty} \frac{\beta(\lambda)}{P+\lambda} d\lambda. \tag{6}$$

Figure 5. Measurement method for impedance (a) $Z_{in,c}(jw)$, (b) $Z_{in,nc}(jw)$.
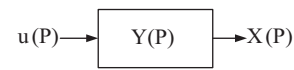
Figure 6. Transfer function Y.

The diffusive realization Y_{diff} of operator Y is the infinite dimensional state representation:

$$\begin{cases} \frac{d\phi(\lambda,t)}{dt} = -\lambda.\phi(\lambda,t) + u(t) \\ X(t) = \int_0^{+\infty} \beta(\lambda).\phi(\lambda,t)d\lambda \\ \lambda > 0, \phi(\lambda,0) = 0 \end{cases} \tag{7}$$

The state representation in Eq. (7) can be approximated with arbitrary precision by discretization of the frequency variable λ, leading by quadrature to realization of finite order K.

$$\begin{cases} \frac{d\phi_j(t)}{dt} = -\lambda_j.\phi_j(t) + u(t), j = 1 \rightarrow K, \phi_j(0) = 0 \\ X(t) = \sum_{j=0}^{K} \beta_j.\phi_j \end{cases} \tag{8}$$

This results in:

$$Z_{diff}(P) = \frac{1}{\sum_{j=1}^{K} \frac{\beta_j}{P+\lambda_j}}. \tag{9}$$

Using the least squares method, an optimal identification of operator Z_{diff} can be obtained. Moreover, diffusive models $Z_{diff,Z}$ and $Z_{diff,G}$ of impedance Z and Z_{Ground} are measured by HP impedance. The Bode diagrams of the measurements taken at 25 are presented in Figures 7 and 8.
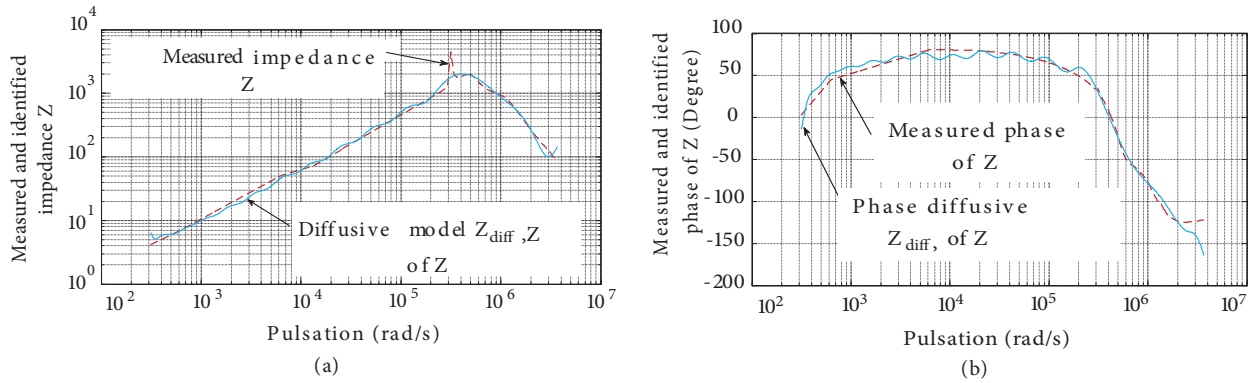
Figure 7. Comparison between measured Z and identified $Z_{diff,Z}$ by diffusive realization:(a) module, (b) phase.
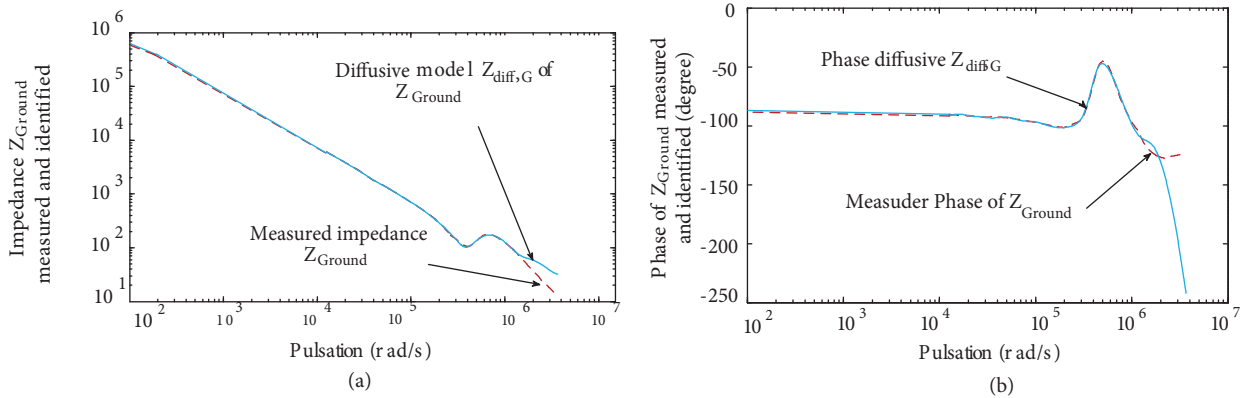

Figure 8. Comparison between the measured Z_{Ground} and identified $Z_{diff,G}$ by diffusive realization: (a) module, (b) phase.

Figure 9 shows the diffusive model of a phase with four coils, which is obtained by replacing Z and Z_{Ground} with $Z_{diff,Z}$ and $Z_{diff,G}$ that was shown earlier in the block diagram shown in Figure 4.

## 4. Thermal model of the permanent magnet synchronous motor

The losses consumed in the motor cause a rise in the temperatures of different parts of the machine. The losses of the machine are evaluated using an electrical model or by measurement, while the distribution of the temperatures in the machine is ascertained via a thermal model. Both models are coupled and parameters of the electrical model are corrected according to the results provided by the thermal model. Figure 10a shows the variation in impedance as a function of frequency and temperature while Figure 10b shows the coupled block diagram of the diffusive models. The model inputs are the sources of the dissipated thermal power PT and the outputs are transient thermal responses to different nodes of the previously-developed circuit model.

Eq. (10) presents the input/output representation for the model thermal diffusive approach.

$$\begin{cases} \frac{d\psi_k(t)}{dt} = -\xi_k.\psi_k(t) + P_T(t) \\ \psi_k(0) = 0 \\ 1 \leq k \leq N \\ \theta_T = \sum_{k=1}^{N} \eta_k.\psi_k \end{cases} . \tag{10}$$
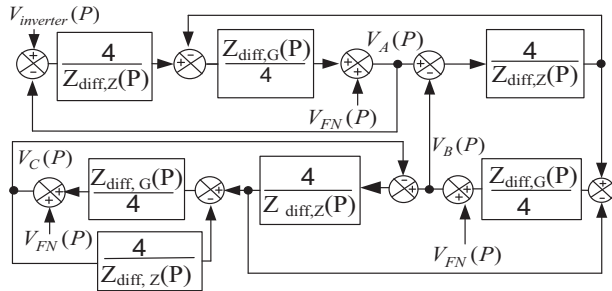
Figure 9. Diffusive model of permanent magnet synchronous motor phase.
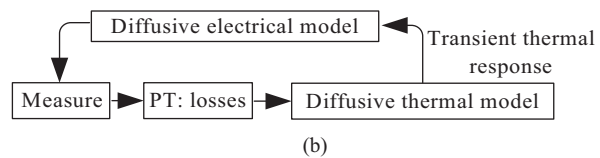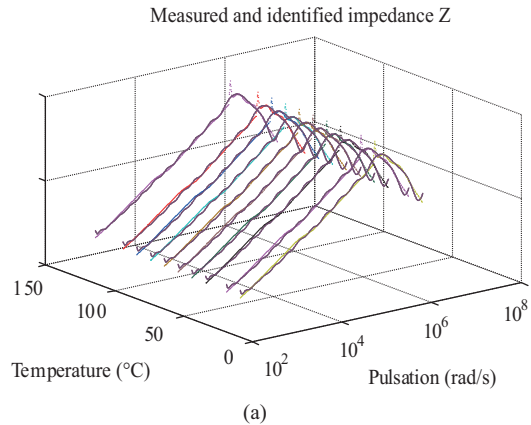
Figure 10. Coupled models: (a) dependence of impedance to frequency and temperature, (b) coupled models between diffusive thermal and electrical.

The significance of the various parameters of the diffusive model equation given in Eq. (10) is as follows:

$(\psi_k)_{k=1\to N}$: the state variables of the diffusive system.

$(\eta_k)_{k=1\to N}$: the diffusive symbol.

$(\xi_k)_{k=1\to N}$: the frequency mesh.

Furthermore, the accuracy of the model mainly depends on the number (ξ_k), whereas distribution of $(\xi_k)_{k=1\to N}$ must take account of the dynamic system. The diffusive parameter identification $(\eta_k)_{k=1\to N}$ and $(\xi_k)_{k=1\to N}$ can be realized by two methods: either by the transfer functions of the system, or on knowing the result of a measurement. The latter method has proven easier than the first, given that optimal identification by least square method can lead to more precise modelling of diffusive thermal transfer.

4.1. Physical dimension of diffusive parameters

The propagation of heat conduction is written as in [23]:

$$\frac{\mathrm{d}\theta_T}{\mathrm{d}t} = -\frac{[G_{eq}]}{[C]}.\theta_T + \frac{1}{[C]}.P_T. \tag{11}$$

The model of thermal diffusive approach is:

$$\begin{cases} \frac{\mathrm{d}\psi}{\mathrm{d}t} = -\xi.\psi + P_T \\ \theta_T = \psi.\eta \end{cases}, \tag{12}$$

$$\frac{\mathrm{d}\theta_T}{\mathrm{d}t} = \eta.\frac{\mathrm{d}\psi}{\mathrm{d}t} = -\eta.\xi.\psi + \eta.P_T = \xi.\theta_T + \eta.P_T. \tag{13}$$

The diffusive parameters η and ξ have physical dimensions.Through the identification between Eqs. (12) and (13), we have:

$$\begin{cases} \xi = -\frac{G_{eq}}{C}[Hz] \\ \eta = \frac{1}{C}[K.J^{-1}] \end{cases} .$$ (14)

4.2. Identification parameter

Knowing only the dissipated power PT and a measure, or an estimation of the output by the FEM, the numerical identification step of the least square method is used to find the parameters $(\eta_k)_{k=1 \to N}$. The temperature measurement provides θ_{mes} at different sampling times δT_{ech}. We select the (ξ_k) distribution to cover the system bandwidth. The distribution range (ξ_k) is limited by the extreme values (ξ_{min}) and (ξ_{max}), which are given by the following equations:

$$\xi_{min} \leq \frac{1}{\tau},$$ (15)

$$\xi_{max} \geq \frac{1}{\delta T_{ech}},$$ (16)

where τ is the thermal time constant and ΔT_{ech} is the sampling pitch. Furthermore, we chose a distribution of (ξ_k) in a geometric distribution of R_{eas} reason, such as:

$$\xi_{k+1} = R_{eas}.\xi_k,$$ (17)

$$R_{eas} = \left(\frac{\xi_{max}}{\xi_{min}} \right)^{\frac{1}{N-1}} .$$ (18)

In the second step, the $(\eta_k)_{k=1 \to N}$ is identified by using the least square method. The solution is presented in Eq. (19):

$$min \sum_{m=1}^{M} (\theta_{mes} - \eta.\psi)^2 .$$ (19)

The problem of finding (η) minimizing the Euclidean distance between (θ_T) and (θ_{mes}) has a unique solution conventionally obtained by:

$$\eta = \left(\psi^t.\psi \right)^{-1} .\psi^t.\theta_{mes},$$ (20)

where ψ^t is the transpose of ψ.

Finally, in order to manage the diffusive identification of the model parameters, we implemented an easy-to-use graphical analysis method as shown in Figure 11. If the identified temperature is not satisfying, the process of identification must be still carried out increasing the order N of system. The model developed is very simple to simulate by a digital simulator such as MATLAB/Simulink. In addition, it is very fast compared with the FEM simulation.

5. Application and validation

The asynchronous machine is fed by a voltage inverter, Leroy Somer UMV 4301 using scalar control strategy. In addition, the rotor is coupled to an electromagnetic brake, which will play the role of the mechanical load. The machine is fed, during 3622s, under constant load equal to half of its nominal power. At this point, our interest is in the temperature in winding heads, in the slot next to the stator iron and the stator iron. The need for an experimental facility consisting of measurement bench is shown in Figure 12.
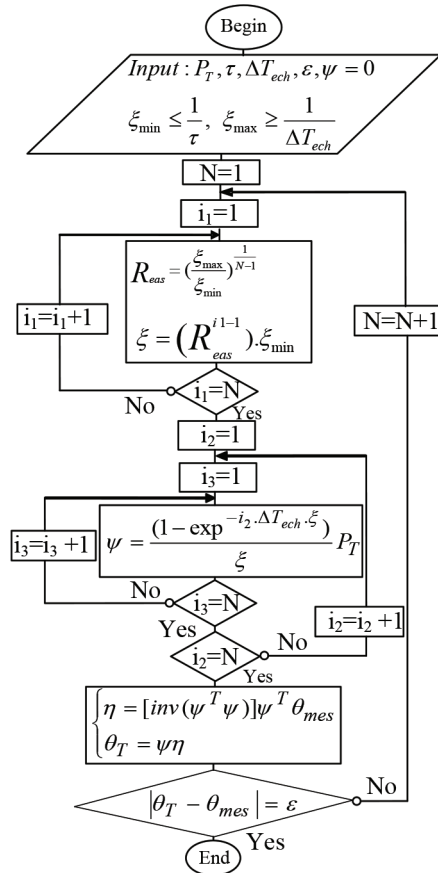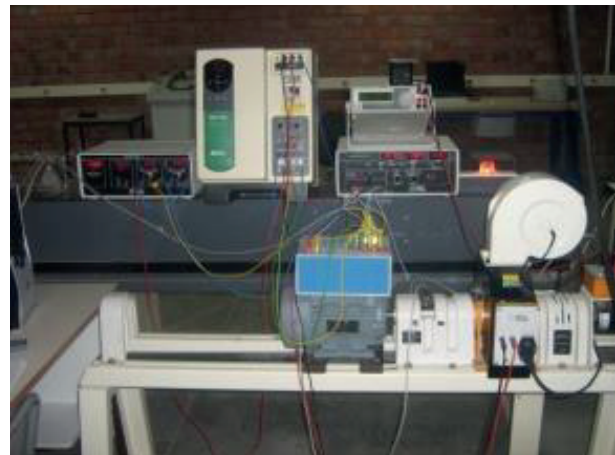

Figure 11. Algorithm of the proposed method.

Figure 12. Measurement bench.

The bench tests include an asynchronous machine instrumented with thermistors, an electromagnetic brake, a voltage inverter, and an acquisition measurement system. Model validation is made by comparison with thermal measurements performed on the machine. The dimension N of the model is nailed when the measurement and the result of the model are identical. Regarding the ratio, R_{eas} of the geometric sequence is fixed after the determination of the good dimension N of the model. The diffusive symbol $(\eta_k)_{k=1 \to N}$ and the frequency base $(\xi_k)_{k=1 \to N}$ are identified by using the method detailed in Section 4. For example, you can use the same time constant τ equal to 1000 s that is deduced by the measure of thermal in each region (stator iron, slot winding, and end winding), while the data sampling rate ΔT_{ech} is equal to 0.01 s. If we have τ and ΔT_{ech}, the maximum and minimum frequency range values are easily calculated by Eqs. (15) and (16). Thereafter, the maximum frequency range (ξ_{max}) is equal to 1000 Hz and the minimum frequency (ξ_{min}) = 10–3 Hz. Finally, the ratio of geometric R_{eas} is calculated using Eq. (18) that is equal to 31.623. Figures 13–15
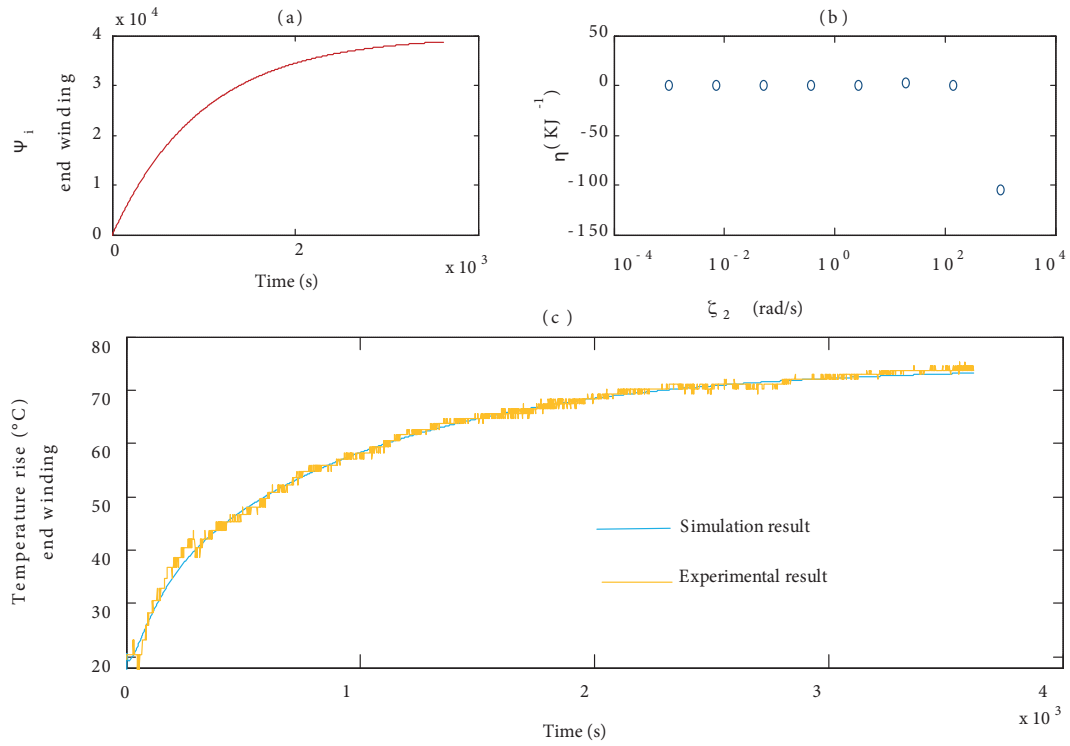
Figure 13. Temperature at end winding: (a) (ψ_1) variation as a function of time, (b) variation of (η_1) according to ξ_1, and (c) validation of the thermal model at the end winding.
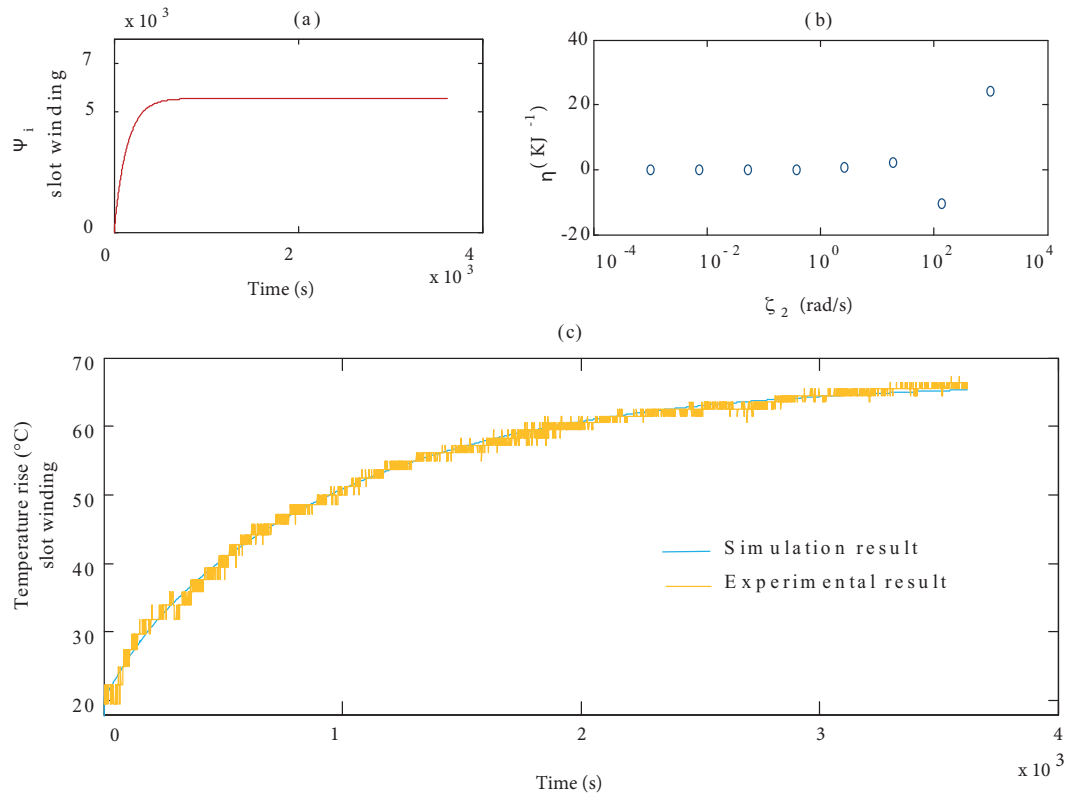
Figure 14. Temperature at slot winding: (a) (ψ_2) variation as a function of time, (b) variation of (η_2) according to ξ_2, and (c) validation of the thermal model at the end winding.

present comparisons between experimental and simulation results for the diffusive thermal model. The results suggest a satisfactory level of accuracy of the developed thermal model.

To validate the diffusive thermal model for different load levels, we performed a test where the motor is fed by the same inverter with variable mechanical load cycles. Figures 16–18 present the simulation of the diffusive thermal model and experimental results for half rated load and for rated load operation. As seen in the figures, the simulation results are in good agreement with the measurement results. Moreover, it can be seen that there is more pronounced variation in temperatures in the end winding and the winding slot than in the stator iron.

In addition, MATLAB/Simulink is used to validate the high frequency modeling of the stator winding developed in Section 3. Figures 19 and 20, present the simulated and measured voltages between the phase 1 and the neutral and across coils A, B, C, and D. Two interesting observations were made during the propagation of the voltage front across the stator winding; the collapse of the applied voltage front and the propagation delay. This is the eddy current induced in the magnetic circuit which is responsible for the collapse of the front. However, the delay is attributed to the time it takes the front through the coil, which depends on the geometric and physical characteristics of the winding. The voltage at the coil terminals depends on the front of voltage and the propagation delay. Beyond the transient regime, the propagation of the voltage is uniform.

## 6. Preventive reactivity and surveillance system

Whether preventive conditional maintenance entails use of tools to facilitate the detection of a failure before it occurs. In some cases, undetected real-time degradation can be catastrophic. The exploitation of previously developed models can be a basis for real-time surveillance of the insulation quality. The supervisory system is based on detecting overvoltage at the terminals of the first coil of each phase. This overvoltage is sensitive to variations in capacitive coupling interturns or interlayers which are the consequences of damage to the dielectric properties of the insulation system. We are considering implementing a diagnostic method presented in Figure 21. In fact, the absence of a signature is based on calculating an error $\epsilon(t)$ between the temporal evolution of the voltage estimated by the mathematical model and the temporal evolution of the voltage measured by a high-band width voltage sensor connected across the first coil. Mathematically, two methods are used to estimate the temporal evolution of the voltage and current at any point in the coil. The first methods consist of applying the inverse Fourier transformation to the transfer function winding and subsequently applying the convolution product with the PWM input signal type. The second approach is to obtain a state model using the Diffusive Representation. The state variables analysis facilitates identifying the elements responsible for the observed overvoltage and studying their sensitivity to various parameters. The winding monitoring strategy is based on analysis of various criteria relating to the estimation error, integral of square error criterion, integral of absolute value of the error criterion, and integral of the time-weighted absolute error criterion. Other criteria could be considered as the voltage rise time and the analysis of the spreading of the wave of the voltage over time. The content and location of the degradation will be determined by assessing the relative importance of all the criteria mentioned above and then adopting a multicriteria analysis approach type analytic, hierarchical process. The responsiveness of our monitoring system entails treating the risk of failure among the turns. This risk is greater for pulses having a very high front dV/dt. To increase the reliability of the machine, developing a modulation technique to reduce overvoltage is considered. Moreover, we can consider implementing a commutation save circuit 'CALC' self-adaptive connected across each power switch to limit the increase of the forward voltage in the off state of the semiconductor. The parameters of the CALC are "self-adaptive" with the content of the degradation of the insulation system.
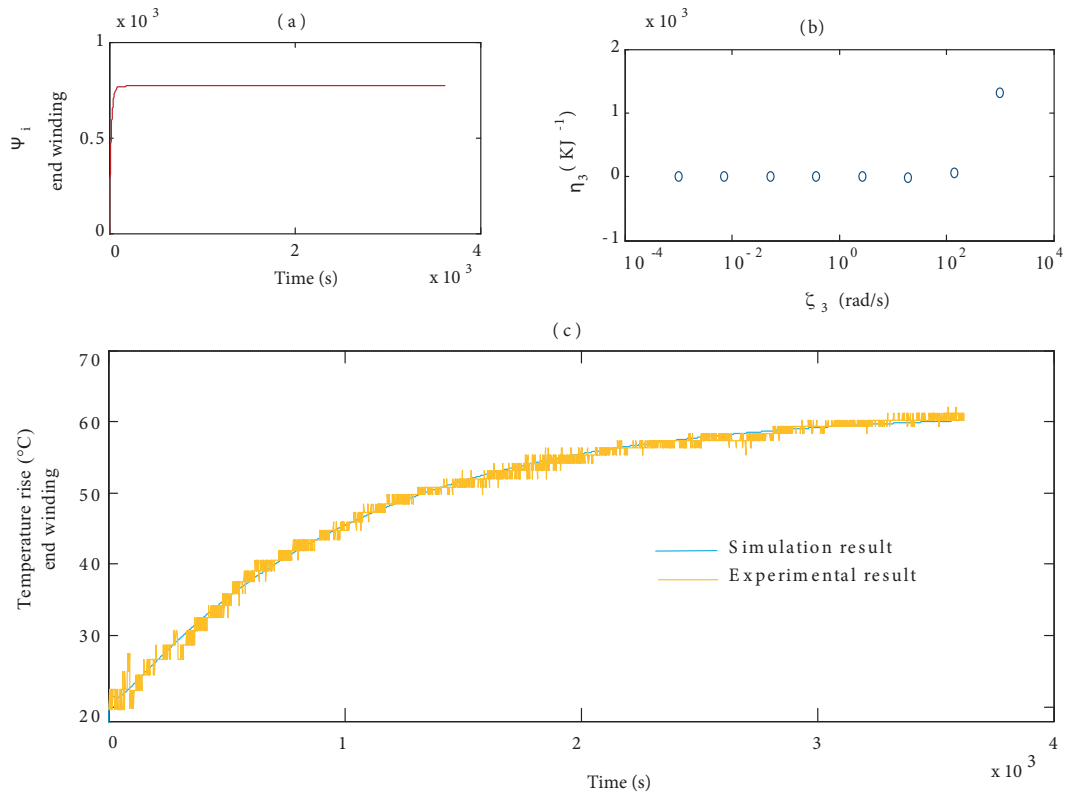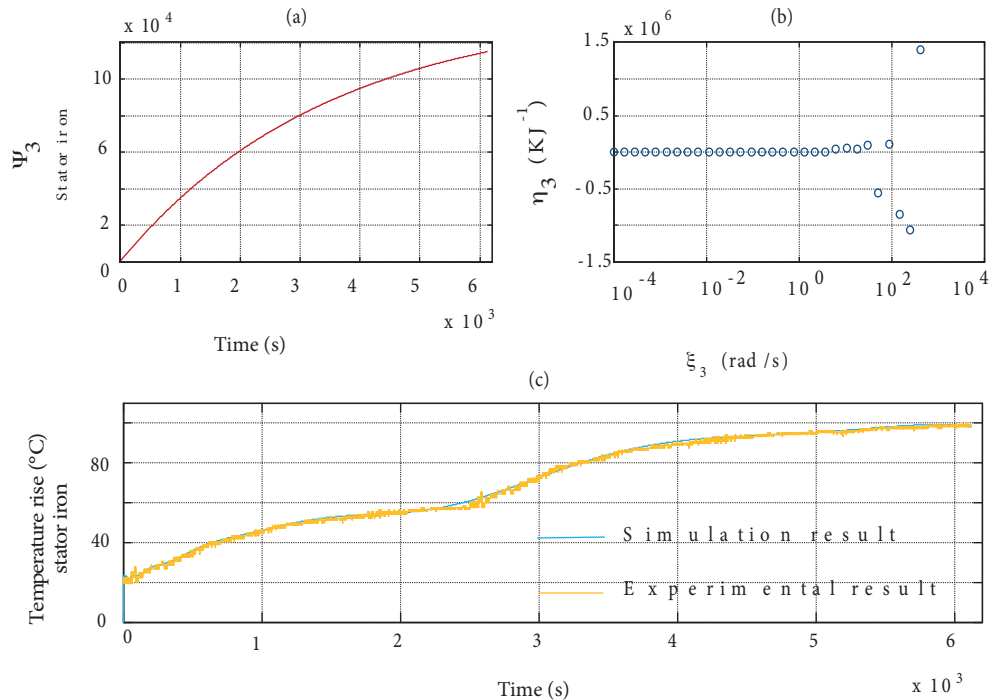
Figure 15. Temperature at stator iron: (a) (ψ_3) variation as a function of time, (b) variation of (η_3) according to ξ_3, and (c) validation of the thermal model at the end winding.
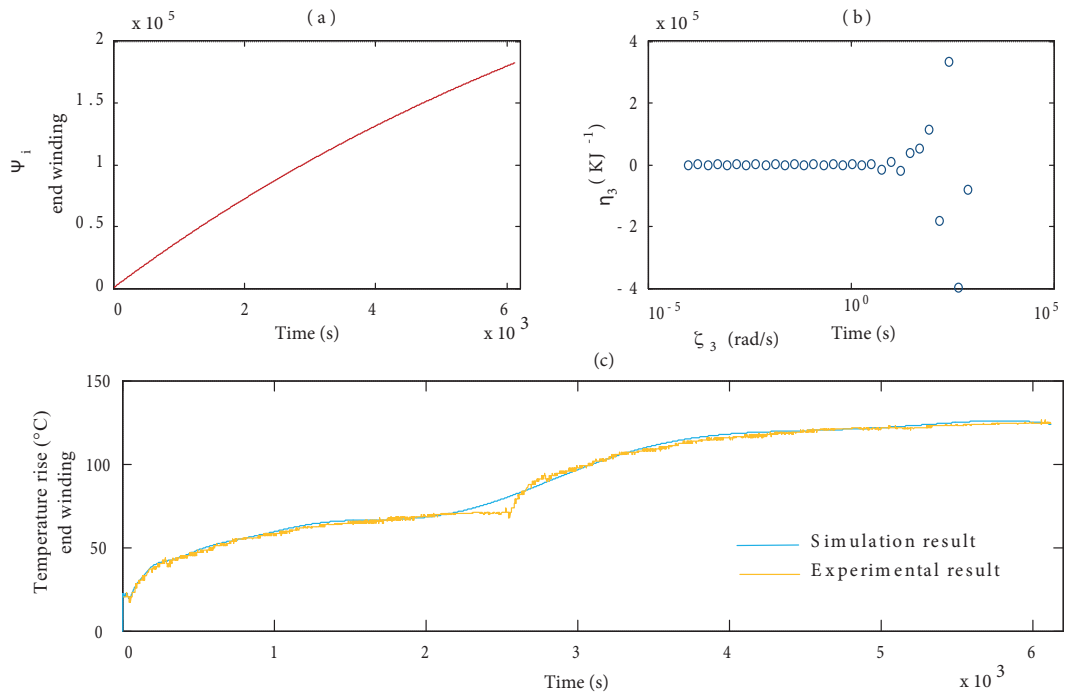
Figure 16. Temperature at end winding: (a) (ψ_1) variation as a function of time, (b) variation of (η_1) according to ξ_1, and (c) validation of the thermal model at the end winding.
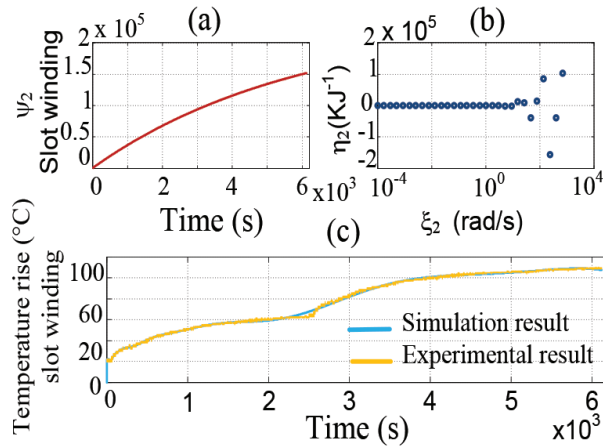
Figure 17. Temperature at slot winding: (a) (ψ_2) variation as a function of time, (b) variation of (η_2) according to ξ_2, and (c) validation of the thermal model at the end winding.

Figure 18. Temperature at stator iron: (a) (ψ_3) variation as a function of time, (b) variation of (η_3) according to ξ_3, and (c) validation of the thermal model at the end winding

7. Conclusion

The goal of the study presented in this paper is to implement a general yet simple methodology to develop both transient thermal and electrical models for permanent magnet synchronous motor, regardless of its geometric complexity and nature of material. Our proposed technique utilizes the compatibility in multiphysics simulators associated with input/output characteristics. We have also proposed the coupled diffusive for thermal and overvoltage distributions when the motor is fed by an inverter. The coupling of a thermal model with an electrical model supports consideration of interactions between electrical and thermal properties as well as
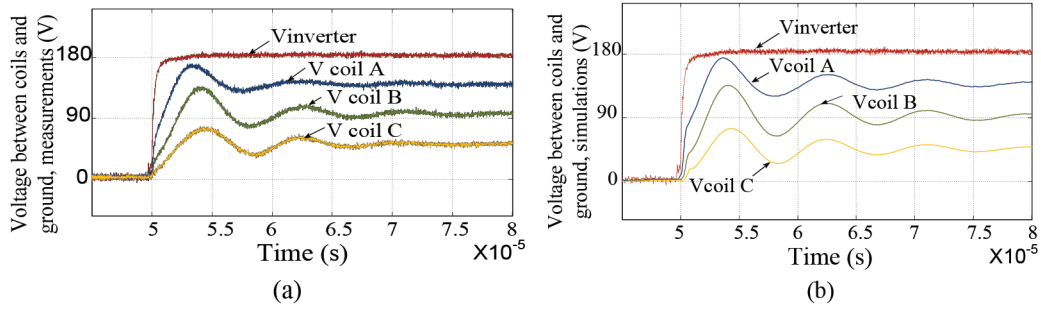
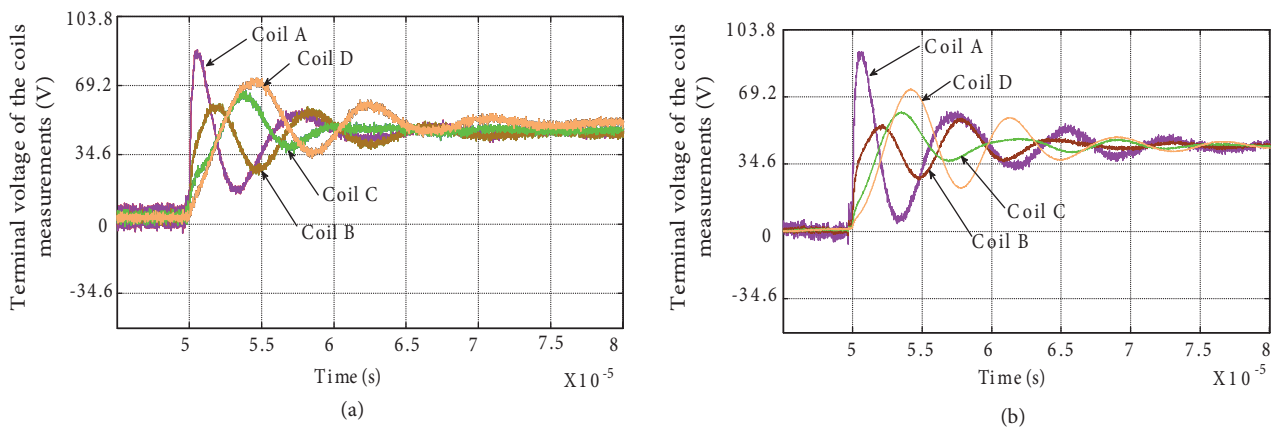**Figure 19**. Coils to ground voltage: (a) measurement, (b) simulations.

Figure 20. Voltage at the coils terminals: (a) measurement, (b) simulations.
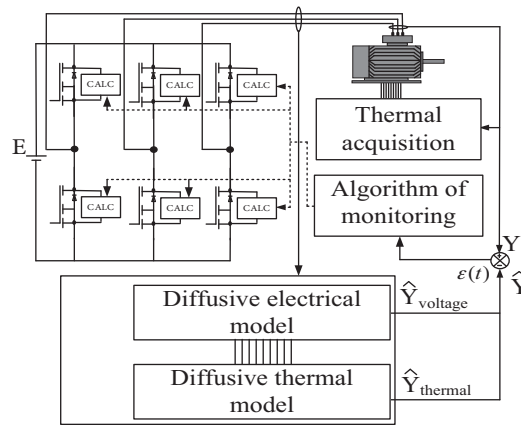

Figure 21. Monitoring system.

modeling of the machine when subjected to variable load torque and when fed by an inverter. Thus, it is possible to provide for the possible derating of the machine and the dimensioning of the converter from the voltages and the current required for supplying the machine.

References

[1] Khaled B S, Bidan P, Lebey T, Ammar F B, Elleuch M. Identification and time domain simulation of the association inverter-cable-asynchronous machine using diffusive representation. IEEE Trans Power Electron 2009; 56: 257-256.

[2] CEI/TS 6003-17. Cage induction motors when fed from converters- Application guide, partie-17, 2006.

[3] Cassat A, Wavre CEN. BLDC motor stator and rotor iron losses and thermal behavior based on lumped schemes. IEEE Trans Ind Appl 2003; 39: 1341-1322.

[4] Zhang P, Du Y, Lu B, Habetler TG. ADC Signal injection-based thermal protection scheme for soft-stater-connected induction motors. IEEE Trans Ind Appl 2009; 5: 1351-1358.

[5] Kral C, Habetler T G, Harley RG, Pirker F, Pascoli G, Oberguggenberger H, Fenz CJM. Rotor temperature estimation of squirrel-cage induction motors by means of a combined scheme of parameter estimation and a thermal equivalent model. IEEE Trans Ind Appl 2004; 40: 1049-1057.

[6] Mendes AMS, Lopez Fernanadez XM, Marques Cardoso AJ. Thermal performance of a three-phase induction motor under fault tolerant operating strategies. IEEE Trans Power Electron 2008; 23: 1537-1544.

[7] De Abreu P G J, Emanuel A E. Induction motor thermal aging caused by voltage distortion and imbalance: loss of useful life an dits estimated cost. IEEE Trans Ind Appl 2003; 38: 12-28.

[8] Boglietti A, Cavagnino A, Lazzari M, Pastorelli M. A simplified thermal model for variable speed self-cooled industrial induction motor. IEEE Trans Ind Appl 2003; 39: 945-952.

[9] Boglietti A, Cavagnino A. Analysis of the endwinding cooling effects in TEFEC induction motors. IEEE Trans Ind Appl 2007; 43: 1214-1222.

[10] Boglietti A, Cavagnino A, Staton DA, Popescu M, Cossar C, Mc Gilp MI. End space heat transfer coefficient determination for different induction motor enclosure types. IEEE Trans Ind Appl 2009; 45: 929-937.

[11] Lee Y, Hahn S Y, Ken Kauh S. Thermal analysis of induction motor with forced cooling channels. IEEE Trans Mag 2009; 36: 1398-1402.

[12] Bianchi N, Bolognani S, Tonel F. Thermal analysis of a run-capacitor single-phase induction motor. IEEE Trans Ind Appl 2003; 39: 457-465.

[13] Staton D A, Cavagnino A. Convection heat transfer and flow calculations suitable for electric machines thermal models. IEEE Trans Ind Electron 2008; 55: 3509-3516.

[14] Boglietti A, Cavagnino A, Parvis M, Vallan A. Evaluation of radiation thermal resistances in industrial motors. IEEE Trans Ind Appl 2006; 42: 688-692.

[15] Gao Z, Colby R S, Habetlerand T G, Harley R G. A model reduction perspective on thermal models for induction machine overload relays. IEEE Trans Ind Electron 2008; 55: 3525-3534.

[16] Alberti L, Bianchi N. A coupled thermal electromagnetic analysis for a rapid and accurate prediction of IM performance. IEEE Trans. Ind. Electron. 2008; 55: 3575-3582.

[17] Marignetti F, DelliColli V, Coia Y. Design of axial flux PM synchronous machines through 3-D coupled electro-magnetic thermal and fluid-dynamical finite-element analysis. IEEE Trans Ind Electron 2008; 55: 3591-3601.

[18] Tenconi A, Profumo F, Bauer SE, Hennen MD. Temperatures evaluation in an integrated motor drive for traction applications. IEEE Trans. Ind. Electron. 2008; 55: 3619-3626.

[19] Han J, Li W, Li Y. Analysis of three dimensional complex fluid flow and temperature distribution in the end region of a turbogenerator. IEEE Trans Ind Electron 2015; 62: 5370-5381.

[20] Jiang W, Jahns T M. Coupled electromagnetic-thermal analysis of Electric machines including transient operation based on finite-element technique. IEEE Trans Ind Appl 2015; 51: 1880-1889.

[21] Buyukdegirmenci VT, Krein PT. Induction machine characterization for short-term or momentary stall torque. IEEE Trans Ind Appl 2015; 51:2237-2245.

[22] Chen Q, Zou Z. Lumped-parameter thermal analysis and experimental validation of interior IPMSM for electrical vehicle. Journal of Electrical Engineering & Technology 2018; 13: 2276-2283.

[23] Zhu S, Cheng M, Cai X. Direct coupling method for coupled field-circuit thermal model of electrical machines. IEEE Trans Ener Conv 2017; 33: 473-482.

[24] Nerg J, Rilla M, Pyrh nen J. Thermal analysis of radial-flux electrical machines with a high power density. IEEE Trans. Ind. Electron. 2008; 55: 3543-3554.

[25] Jungreuthmayer C, Bauml T, Winter O, Ganchev M, Kapeller H, Haumer A, Kral C. A detailed heat and fluid flow analysis of an internal permanent magnet synchronous machine by means of computational fluid dynamics. IEEE Trans Ind Electron 2012; 59: 4568-4578.

[26] EL-Refaie A M, Harris N C, Jahns T M, Rahman K. Thermal analysis of multibarrier interior PM synchronous machine using lumped parameter model. IEEE Trans Energy Convers 2004; 19: 303-309.

[27] Han PW, Choi JH, Kim D J, Chun JY, Bang DJ. Thermal analysis of high speed induction motor by using lumped-circuit parameters. Journal of Electrical Engineering & Technology 2015; 10: 2040-2045.

[28] Mellor PH, Roberts D, Turner DR. Lumped parameter thermal model for electrical machines of TEFC design. IEEE Proceedings-B 1991.

[29] Staton DA, Cavagnino A. Convection heat transfer and flow calculations suitable for electric machines thermal models. IEEE Trans Ind Electron 2008; 55: 3509-3516.

[30] Howey DA, Childs PRN. Air-gap convection in rotating electrical machines. IEEE Trans Ind Electron 2012; 59: 1367-1375.

[31] Marignetti F, Colli V D, Coia Y. Design of axial flux PM synchronous machines through 3-D coupled electromagnetic thermal and fluid-dynamical finite-element analysis. IEEE Trans Ind Electron 2008; 55: 3591-3601.

[32] Marignetti F, Delli Colli V. Thermal analysis of an axial flux permanent-magnet synchronous machine. IEEE Trans Magn 2009; 45: 2970-2975.